Supplementary Information:

Future methane, hydroxyl, and their uncertainties: key climate and emission parameters for future predictions

Christopher D. Holmes [1*], Michael J. Prather [1], Amund O. Søvde [2], Gunnar Myhre [2]

[1] Department of Earth System Science, University of California, Irvine, CA 92697-3100 USA

[2] Center for International Climate and Environmental Research (CICERO), Oslo, Norway

[*] Correspondence to cdholmes@uci.edu

Methyl chloroform decay rate and its uncertainty

The AGAGE network consists of 5 sites, each of which makes measurements every 20 minutes, with analysis and calibration done on site. In the NOAA network, flasks are filled 1-4 times monthly and analyzed in a central laboratory in Boulder, Colorado. To avoid pollution influences, flasks are filled when winds blow from a clean sector. In the AGAGE network polluted samples are identified as anomalously high MCF concentrations and removed from analysis.

Both networks provide monthly average data for each of their sites, which we use here (NOAA: ftp://ftp.cmdl.noaa.gov/hats/solvents/CH3CCl3/flasks/GCMS/CH3CCL3_GCMS_flask.txt, accessed Aug 6, 2012; AGAGE: http://agage.eas.gatech.edu/data_archive/agage/gc-md/monthly/, accessed April 4, 2012). For the NOAA network, we use data from the same 9 sites as Montzka et al. (2011) (South Pole; Cape Grim, Australia; Cape Matatula, American Samoa; Alert, Canada; and United States sites at Mauna Loa, Hawaii; Niwot Ridge, Colorado; WLEF tower, Wisconsin; and Barrow, Alaska). All 5 AGAGE sites are used here analysis (Cape Grim, Australia; Cape Matatula, American Samoa; Ragged Point, Barbados; Trinidad Head, United States; and Mace Head, Ireland). NOAA data are truncated at December 2007 due to later quality issues (S. Montzka, pers. comm.).

Our method for calculating the global MCF decay rate differs from that of Montzka et al. (2011). Montzka et al. first constructed a global mean tropospheric MCF abundance from a weighted average of the sites, then calculated the global decay rate using the same formula we have applied to each site individually. We find our method to be much less sensitive to site selection and methods for filling missing data, but our global mean decay rates and their anomalies are, nevertheless, very similar, as shown in Figure S1. Differences are always less than 1% after 2000, but are as large as 2% in early 1998, due to more frequent data gaps in the early period.

The standard error in the mean, *s*, for NOAA sites is calculated as $s = \sigma/\sqrt{N}$, where σ is the standard deviation of the *N* samples during each month. While NOAA sites make 1-4 measurements monthly, AGAGE sites make hundreds, introducing significant autocorrelation. We find that the AGAGE data are well-fit by a first-order autoregressive model. The standard error in the mean for a first-order autoregressive time series is $s = \sigma/\sqrt{N}\ \sqrt{(1+\rho)/(1-\rho)}$,

where ρ is the first-order auto regressive coefficient, which varies seasonally and between years (see e.g. Wilks 2006, Section 8.3.5). Adopting ρ = 0.75, the highest value for any 1-month period at any AGAGE site since 2000, provides an upper limit on the standard error in the monthly means. The monthly mean MCF concentrations measured at collocated NOAA and AGAGE stations frequently differ by more than their standard errors (Figure S2).

Future tropospheric temperature and water vapor

The parametric model for $\tau_{CH4\times OH}$ requires global-mean atmospheric temperature and water vapor as inputs. These input data must be consistent with other scenario emission data, which are taken from RCP 8.5 in this work. Since surface temperature data are easily available from CMIP5 models, we derive future atmospheric temperature and water vapor from surface temperature in CMIP5 models, using historical correlations between these climate variables.

Figure S3 shows strong correlations between historical (1979-2010) surface temperature and tropospheric temperatures. These correlations are robust against different meteorological analysis products (R^2=0.6 to 0.8). Using MERRA data (Bosilovich et al., 2011) since 1979, the slope of atmosphere vs. surface temperatures is 0.94 ± 0.1. ECMWF data (cycle 36r1, (Prather et al., 2012)) since 1997 yield a statistically indistinguishable value from MERRA data over the same period.

Water vapor mixing ratio can be calculated from atmospheric and surface temperatures using standard vapor pressure formulas (e.g. Eq. 2.61 Jacobson, 2005), assuming constant relative humidity. Figure S4 shows that the calculated water vapor is highly correlated with reanalysis water vapor (R^2 = 0.65-0.85) with a slope of 1.5 ± 0.1 when the calculations are based on surface temperature. The slope deviates from 1:1 because both temperature and water vapor are averaged globally, while vapor pressure formulas strictly apply only to homogeneous regions.

An ensemble of 35 CMIP5 models provide global surface temperature predictions for RCP 8.5 climate (Climate Explorer, http://climexp.knmi.nl/, accessed December 18, 2012). We calculate future atmospheric temperature, $T_i(t)$ in each model i to be

$T_i(t) = T_0 + a_1 * [T_{Si}(t) - T_{Si}(t_0)]$,

Where $T_{Si}(t)$ is the model's global mean surface temperature, t_0 = 2010, T_0 = 251.9 K (ECMWF 2000-2009 mean), and $a_1 = N(0.94, 0.1)$ is a normally distributed random number that accounts for uncertainty in the historical fit between atmospheric and surface temperatures. Future water vapor mixing ratio, $q_i(t)$, in the same model is

$q_i(t) = q_0 * \{1 + a_2 * [\, p(T_i(t)) - p(T_i(t_0)) \,] / p(T_i(t_0)) \}$,

where $p(T)$ is the saturation vapor pressure at temperature T, q_0 = 2.45 g kg^{-1} (ECMWF 2000-2009 mean), and $a_2 = N(1.5, 0.1)$ accounts for uncertainty in the historical fit between water vapor and its temperature-derived estimate. Through 10^5 monte carlo realizations of a_1 and a_2 we estimate uncertainty in atmospheric future temperature and water vapor in RCP 8.5.

Figure S5 shows the air temperature and water vapor changes inferred from the surface temperature data. Surface and air temperatures increase 3.8 ± 0.8 K and 3.6 ± 0.9 K, respectively, by 2100 in RCP 8.5. Meanwhile, water vapor increases 43 ± 9.5 % over the same period.

References

Bosilovich, M. G., Robertson, F. R. and Chen, J.: Global Energy and Water Budgets in MERRA,

J Climate, 24(22), 5721–5739, doi:10.1175/2011JCLI4175.1, 2011.

Jacobson, M. Z.: Fundamentals of Atmospheric Modeling, 2nd ed. Cambridge University Press, Cambridge, UK. 2005.

Montzka, S. A., Krol, M., Dlugokencky, E., Hall, B., Joeckel, P. and Lelieveld, J.: Small Interannual Variability of Global Atmospheric Hydroxyl, Science, 331(6013), –, doi:10.1126/science.1197640, 2011.

Wilks, D. S.: Statistical Methods in the Atmospheric Sciences, 2nd Edition, Academic Press, New York, United States, 2006.

Table S1. CTM summary

Model	Meteorology	Resolution	Tropospheric gas species/reactions	Tropospheric aerosols	Heterogeneous chemistry	Photolysis ozone/aerosols[a]	Stratospheric chemistry
UCI CTM	ECMWF cycle 36r1	T42[b]	33/84	None	No	Online/none	Linoz
Oslo CTM3	ECMWF cycle 36r1	T42[b]	51/105	Sulfate, nitrate, sea salt	Yes	Online/none	Online
GEOS-Chem[c]	NASA GEOS-5	2°×2.5°	104/236	Sulfate, nitrate, ammonium, sea salt, dust, OC, BC	Yes	TOMS/online	Linoz

[a] Sources for stratospheric ozone and tropospheric aerosols used in photolysis calculations by Fast-JX.
[b] approximately 2.8°×2.8° at the equator
[c] All sensitivity tests are done with the model as described. We also compare to a simulation using MERRA meteorology at 4°×5° resolution.

Table S2: CTM simulations[a]

Description or perturbed variable	Perturbation		
	Magnitude	Region	Duration, yr
Control simulation, no perturbations	-	-	UCI, CTM3: 13 GEOS-Chem MERRA: 13 GEOS-5: 6
Air temperature in chemistry solver	+1 K	global[c]	3
Water vapor in chemistry solver	+5 %	global[c]	3
Ozone column in photolysis code	+1 %	40°S-40°N	3
Biomass burning emissions	+5 %	global	3 (13 for UCI)
Biomass burning emissions at ground level[d]	-	-	3 (CTM3 only)
Biomass burning emissions at ground level[d]	+5%	global	3 (CTM3 only)
Lightning NOx emissions	+20 %	global	3
Simultaneous air temperature, water vapor, ozone column, biomass burning emissions, lightning NOx emissions	as above	as above	3 (UCI only)
Anthropogenic NOx emissions over land	+7.8 %[b]	global	3
Anthropogenic NOx emissions from ships	+14.4%[b]	global	3
Anthropogenic CO emissions	+5%	global	3
CH_4 abundance	+5 %	global	13
Convective mass flux	–20 %	global	3 (UCI only)
Cloud optical depth (all clouds) in photolysis code	+5 %	global	3 (UCI only)
Cloud optical depth (ice clouds) in photolysis code	+5 %	global	3 (UCI only)
Cloud optical depth (liquid clouds) in photolysis code	+5 %	global	3 (UCI only)

[a] Each variable is perturbed in a separate simulation. All perturbation tests are compared against a control run from the same CTM, except for the two Oslo CTM3 simulations of biomass burning emission altitude, which are compared to each other. GEOS-Chem perturbation tests use GEOS-5 meteorology only.

[b] This magnitude is the projected increase during the period 2000-2030 in RCP 8.5.

[c] In Oslo CTM3, temperature and water vapor perturbations are applied only to grid levels below 200 hPa to avoid confounding effects on stratospheric chemistry.

[d] In the control simulation, Oslo CTM3 emits biomass burning gases and aerosols following the RETRO vertical distribution, which injects 35% of tropical emissions and 45% of boreal emissions above 2 km. For comparison to the other CTMs that put all biomass burning in the boundary layer, we perform two sensitivity simulations in Oslo CTM3 with all biomass burning emitted into the surface layer.

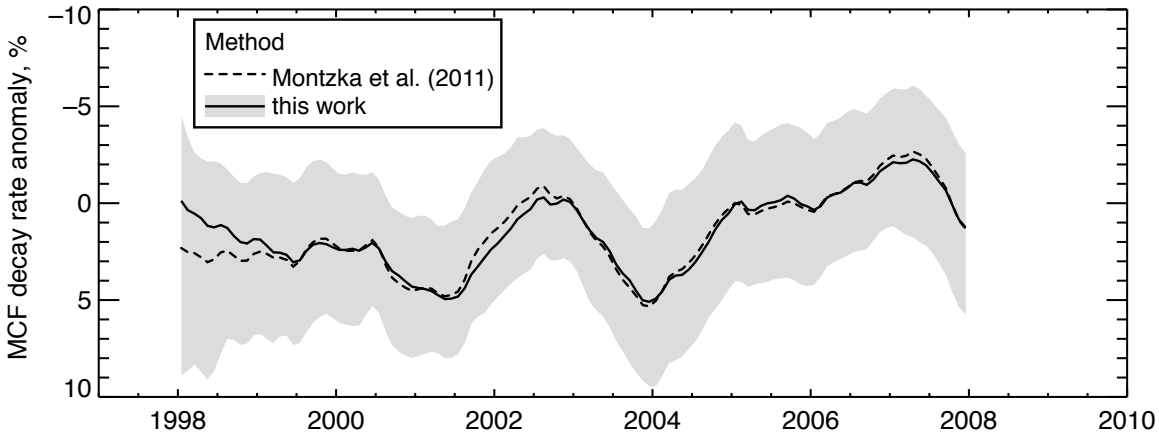

Figure S1. Global decay rate anomalies for methyl chloroform, calculated from NOAA data using two methods. Results from this work are compared to previously published work of Montzka et al. (2011). Shading shows the uncertainty, given by the 16th to 84th percentile range of decay rates across stations within each network, calculated in this work.

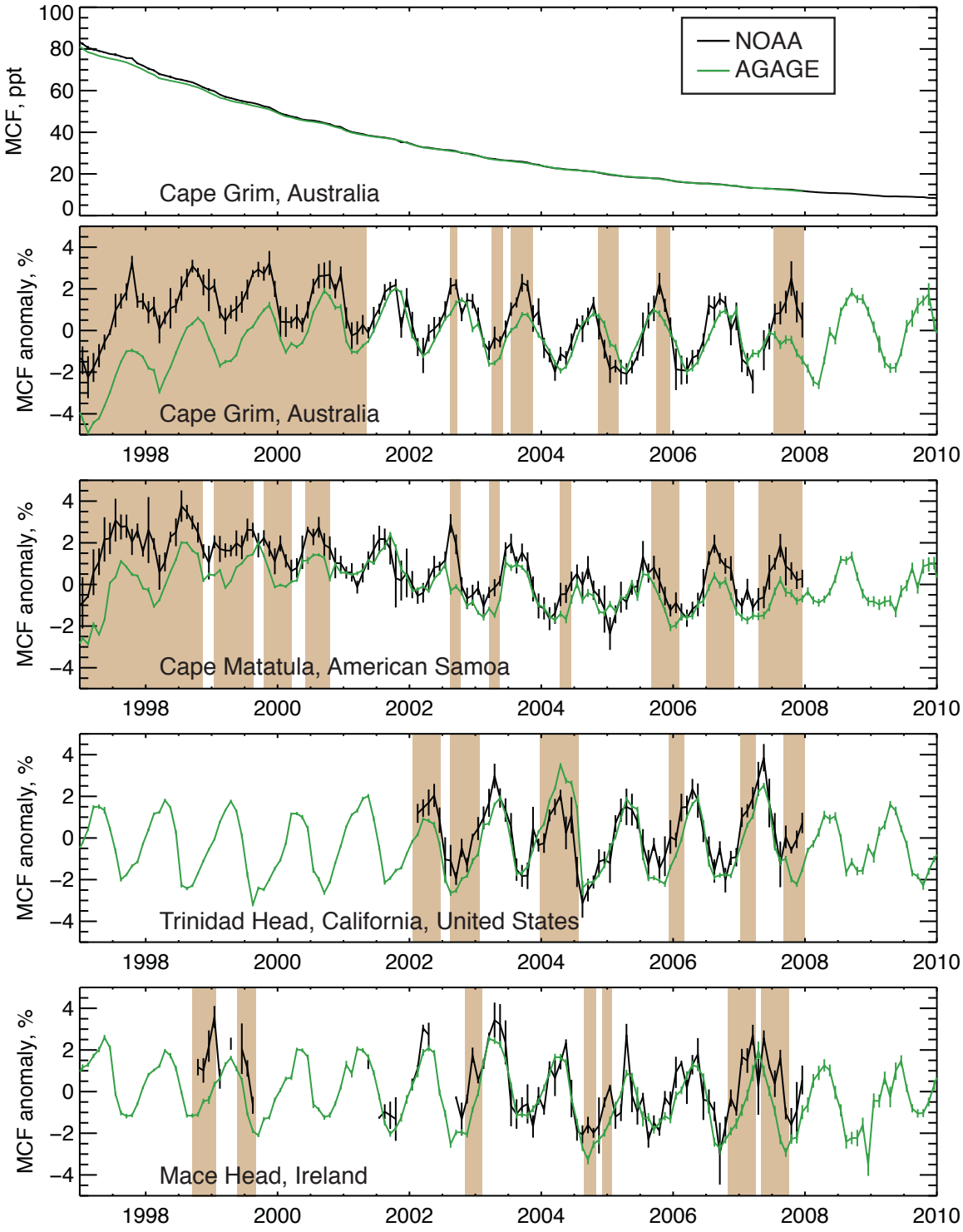

Figure S2. Methyl chloroform (MCF) abundance (top panel) and abundance anomalies (other panels) at sites with collocated NOAA and AGAGE stations. For each collocated station pair, anomalies are calculated with respect to a single decaying exponential reference curve that is fitted to all observations after 2000. Vertical lines show standard errors in the monthly mean abundances. Shading highlights episodes were the NOAA and AGAGE monthly means differ by more than their standard errors for 2 or more consecutive months.

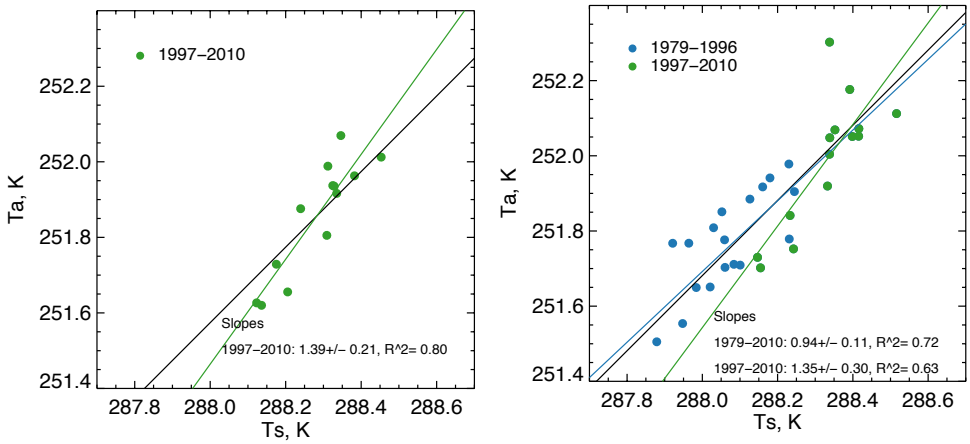

Figure S3. Annual mean atmospheric temperatures (T_a) and surface temperatures (T_S) for ECMWF (left) and MERRA (right) meteorological analyses. Black line shows 1:1 relation. Blue and green lines are ordinary least squares regressions for all years and 1997-2010, respectively.

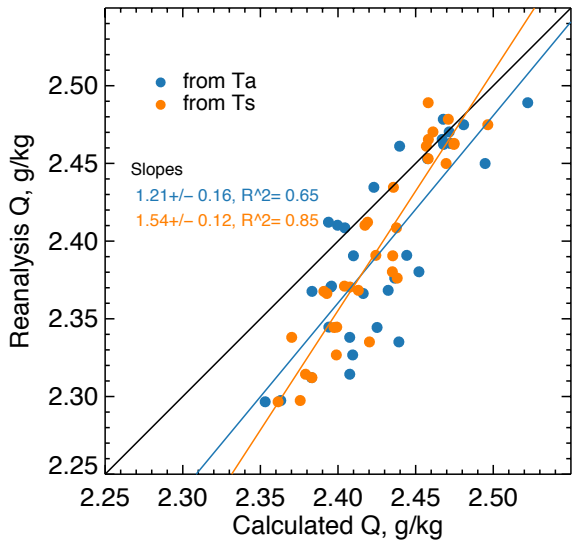

Figure S4. Global mean water vapor mixing ratio from MERRA reanalysis (1979-2009) and calculated from temperature. Calculations are based on either global mean surface temperature (T_S, orange dots) or atmospheric temperature (T_a, blue dots) from MERRA reanalysis, using standard vapor pressure formulas, assuming constant relative humidity. Calculated values are scaled to have the same mean as the reanalysis during 1997-2009.

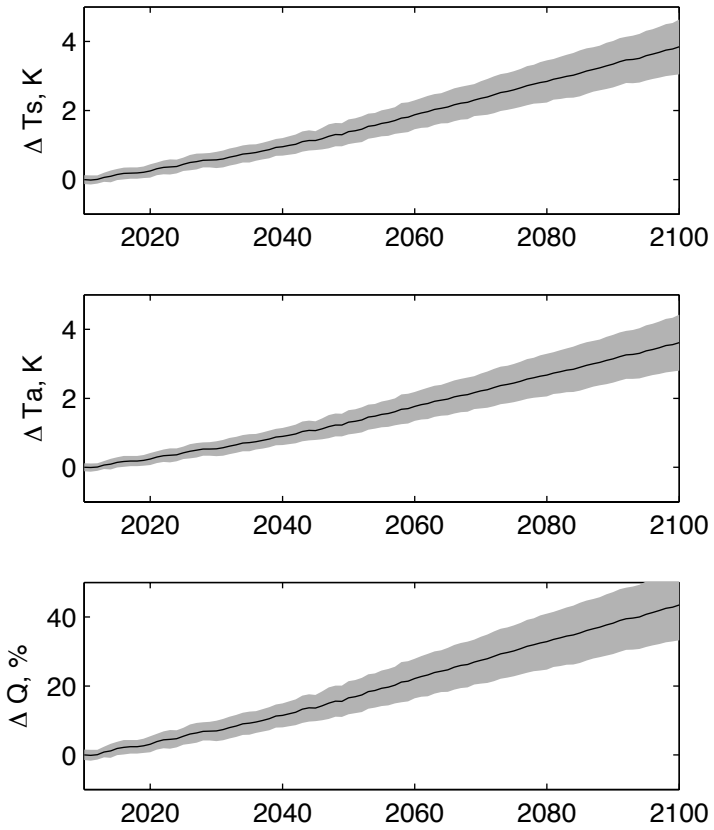

Figure S5. Predicted anomalies in global-mean surface temperature (T_S, top), atmospheric temperature (T_a, middle), and water vapor (Q, bottom) for RCP 8.5. Surface temperatures are from an ensemble of 35 CMIP5 models, while other variables are derived from T_S, as described in this supplement. Shading shows 1σ uncertainty.

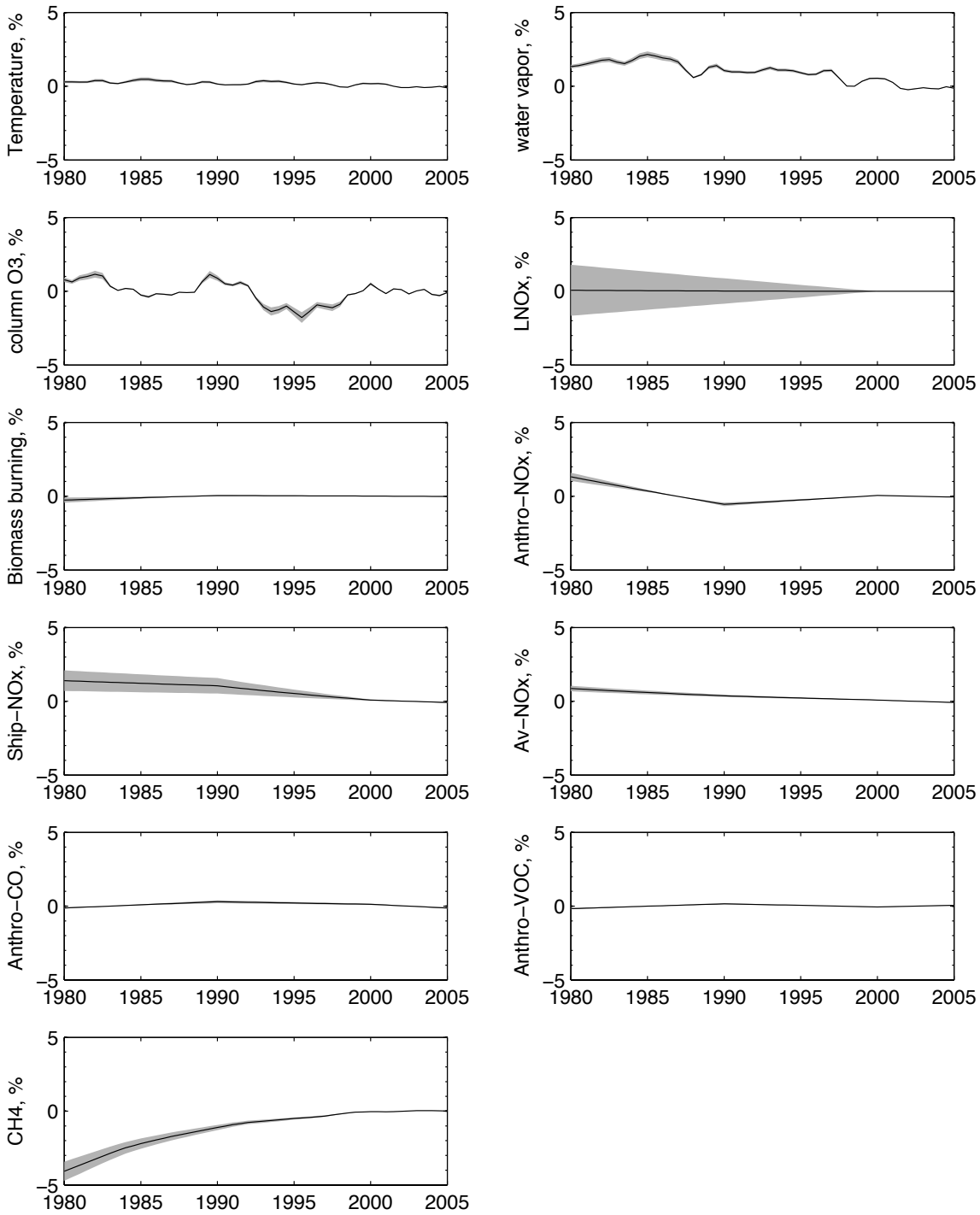

Figure S6. Contributions of climate and emission forcing variables to changes in $\tau_{CH4\times OH}$ since 1980. The sum of all contributions equals the change in lifetime shown in Figure 5.